Electronic properties, Spectroscopic and Biological Investigations of antibacterial active molecule N,N,N',N'- Tetramethylethylenediamine – A DFT Approach

G.Bagavathi Sankar[1], D.Usha[2]

[1]Reg.No18223282131003, Department of Physics, St.Johns College of Arts and Science Ammandivilai

[2]Associate Professor, Department of Physics, Womens Christian College, Nagercoil-629001

[1,2]Affiliated to Manonmaniam Sundaranar University, Abishekapatti, Tirunelveli-627 012, Tamilnadu, India

Abstract

The present paper investigation the biological properties of N,N,N',N'- Tetramethylethylenediamine. The optimized geometry, NBO analysis, Charge analysis were calculated by the B3LYP/6-31G(d,p) level. The spectral analysis has been implemented using FT-IR, FT-Raman, and UV-Visible absorption spectroscopic techniques. Vibrational spectral assignments have been performed using MOLVIB program with potential energy distribution values calculated by normal coordinate analysis. Antimicrobial testing was performed to investigate the compound's efficacy against bacterial strains. To investigate drug likeness was used to determine the biological characteristics of the title molecule. NTE was screened for its antimicrobial activity and found to exhibit antibacterial effects.

Keywords: Antibacterial; DFT; drug likeness; FT IR; Raman; Reduced Density gradien**..**

1. Introduction

More than a few classes of antimicrobial compounds are at the moment existing microorganism's resistance to these drugs continuously rising. With the purpose of avoid this serious health trouble, the embellishment of novel types of antibacterial or antifungal agents or the development of bioactivity of the unsurprisingly known biological active compounds is a very interesting research problem. Diamines contain numerous developed appliances as mechanism of surfactants, pharmaceuticals, agrochemicals, polyamides, and additional materials. Putrescine (1,4-diaminobutane) be presently used toward synthesize nylon-4,6 by polycondensation through adipic acid. 1,4-Butanediamine is in nature biosynthesized in E. coli and is attention to participate a position in cell proliferation and normal cell growth; however, its intracellular concentration in E. coli is highly synchronized by uptake, biosynthesis, degradation, and excretion[1]. The methyl group plays a vital role in the rational drug intend. Methyl improves the metabolic stability as a soft metabolic point. Also, introducing methyl into drug molecules can also be applied as a strategy in new uses of old drugs drugs [2]. Methylene is used in the treatment of drug-induced, suitable to the peculiar reactivity and structural diversity; active methylene compounds comprise a lot of purpose in organic synthesis [3]. N,N,N',N'-Tetramethylethylenediamine is an biological active compound. The aim of this analysis is to evaluate the biological activity with the aid of DFT computations. In order to better understand the structure-activity relationship, and explored using DFT, spectroscopic and bioactivity. The complete spectroscopic vibrational investigation of the molecule is carried out in order to provide a detailed assignment of fundamental bands in the FT-IR, FT-Raman spectrum based on normal coordinate analysis (NCA). The study of frontier molecular orbitals has been used to represent charge transfer in molecules. The antimicrobial activity together with the extensive analysis of the quantum chemical studies, structural characteristics, and electronic properties are discussed in detail.

2. Experimental Details

FT-IR spectrum was recorded using Perkin Elmer Spectrometer with KBr pellet method. FT Raman spectrum was recorded with BRUKER RFS 27: Stand alone FT Raman Spectrometer besides the laser source used was Nd: YAG 1064 nm. UV absorption spectrum in water as a solvent is scrutinized in the range 100-400 nm using Cary 5E UV-Vis NIR recording spectrometer. The antimicrobial activity of NTE was screened by agar well diffusion method and it was tested against four human pathogenic microorganisms were observed and the diameter of the inhibition zone was measured around the well.

3. Computational Details

DFT computations have been implemented using the Gaussian'09 program [4] and the geometry was optimized at B3LYP level with 6-31 G (d, p) basis set. The vibrational spectral modes were assigned with potential energy distribution (PED) values attained from normal coordinate analysis (NCA) using MOLVIB program version 7.0 program by Sundius [5, 6]. The calculated harmonic vibrational

wavenumbers were scaled with multiple scaling factors to present the anharmonicity and accurate the basis set [7]. Natural bond orbital (NBO) analysis were executed using NBO 3.1 program [8]. Reduced density gradient (RDG) analysis, Interaction region indicator (IRI) analysis, Electron Localization function (ELF) and Localized orbital locator (LOL) were performed using Multiwfn, which is a multifunctional wave function analysis program [9,10] and all isosurface maps were rendered by the VMD (Visual Molecular Dynamics) program [11].

4. Results and Discussion

4.1 Optimized Geometry

The optimized geometry was obtained by DFT at B3LYP level with 6-31G(d,p) basis set. The optimized molecular structure is given in Figure 1 and the geometrical parameters of NTE are listed in Table 1.
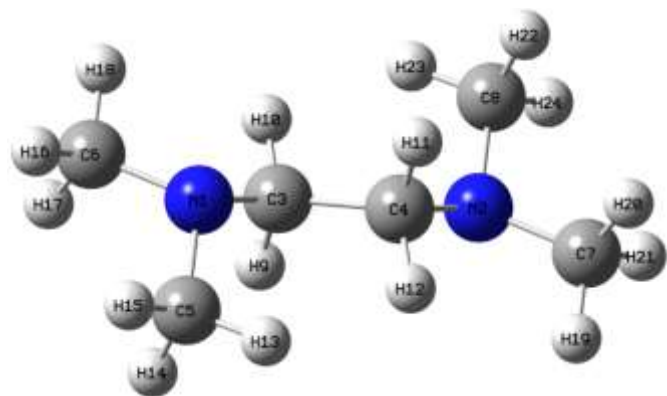

Fig. 1 Optimized structure of NTE

The global minimum energy is -347.7660 Hatrees. Bond length of C5-H14, C6-H17, C7-H20, C8-H22 in methyl group is higher than (1.1079Å) other bond length in methyl group (1.09 Å) in which correlates with the charge transfer from the to the side chain and also the dependency of the side chain length. Skeleton C-C bonds C21-C22 is 1.5347 Å is leads to decrease in bond order and bond energy due to attachment of methyl group and also these relates with the charge transfer to the side chain and also the necessity of the side chain length. Side chain functionalized as a high stability which is observed with carbon atoms in methyl group than other carbon atoms indicating a prominent decrease in electron density.

Table 1 Optimized parameters of NTE

Bond length	NTE(Å)	Bond Angle	NTE(°)	Dihedral Angle	NTE(°)
N1-C3	1.4643	C3-N1-C5	112.8254	C5-N1-C3-C4	-73.4672
N1-C5	1.4579	C3-N1-C6	111.5568	C5-N1-C3-H9	49.8504
N1-C6	1.4572	C5-N1-C6	110.5363	C5-N1-C3-H10	166.6269
N2-C4	1.4644	C4-N2-C7	111.5738	C6-N1-C3-C4	161.3979
N2-C7	1.4572	C4-N2-C8	112.8167	C6-N1-C3-H9	-75.2845
N2-C8	1.4579	C7-N2-C8	110.5318	C6-N1-C3-H10	41.492
C3-C4	1.5347	N1-C3-C4	112.495	C3-N1-C5-H13	59.361
C3-H9	1.1068	N1-C3-H9	112.4424	C3-N1-C5-H14	-61.9397
C3-H10	1.0948	N1-C3-H10	107.0802	C3-N1-C5-H15	177.6677
C4-H11	1.1068	C4-C3-H9	108.8439	C6-N1-C5-H13	-174.9518
C4-H12	1.0948	C4-C3-H10	109.1445	C6-N1-C5-H14	63.7476
C5-H13	1.0929	H9-C3-H10	106.6128	C6-N1-C5-H15	-56.645
C5-H14	1.1079	N2-C4-C3	112.4698	C3-N1-C6-H16	-176.3272
C5-H15	1.0946	N2-C4-H11	112.4453	C3-N1-C6-H17	63.1653
C6-H16	1.0949	N2-C4-H12	107.0862	C3-N1-C6-H18	-57.841
C6-H17	1.1077	C3-C4-H11	108.8482	C5-N1-C6-H16	57.2744
C6-H18	1.0945	C3-C4-H12	109.1509	C5-N1-C6-H17	-63.2331
C7-H19	1.0945	H11-C4-H12	106.6202	C5-N1-C6-H18	175.7606
C7-H20	1.1077	N1-C5-H13	110.8095	C7-N2-C4-C3	-161.1279
C7-H21	1.095	N1-C5-H14	113.0839	C7-N2-C4-H11	75.5659
C8-H22	1.1079	N1-C5-H15	109.4938	C7-N2-C4-H12	-41.225
C8-H23	1.0929	H13-C5-H14	107.9064	C8-N2-C4-C3	73.7366
C8-H24	1.0946	H13-C5-H15	107.4154	C8-N2-C4-H11	-49.5696
		H14-C5-H15	107.9325	C8-N2-C4-H12	-166.3605
		N1-C6-H16	109.6604	C4-N2-C7-H19	57.8577
		N1-C6-H17	113.4976	C4-N2-C7-H20	-63.1549
		N1-C6-H18	109.9237	C4-N2-C7-H21	176.3421
		H16-C6-H17	107.7143	C8-N2-C7-H19	-175.746
		H16-C6-H18	107.9153	C8-N2-C7-H20	63.2413
		H17-C6-H18	107.9552	C8-N2-C7-H21	-57.2616
		N2-C7-H19	109.9266	C4-N2-C8-H22	62.0369
		N2-C7-H20	113.4979	C4-N2-C8-H23	-59.2528
		N2-C7-H21	109.6586	C4-N2-C8-H24	-177.564
		H19-C7-H20	107.9583	C7-N2-C8-H22	-63.6626
		H19-C7-H21	107.9133	C7-N2-C8-H23	175.0477
		H20-C7-H21	107.7116	C7-N2-C8-H24	56.7365
		N2-C8-H22	113.0786	N1-C3-C4-N2	-179.7601

	H11			
n 1(N 2)	σ*C 7 - H19	1.34	0.68	0.028
n 1(N 2)	σ*C 7 - H20	8.54	0.65	0.068
n 1(N 2)	σ*C 7 - H21	1.30	0.68	0.027
n 1(N 2)	σ*C 8 - H22	8.47	0.65	0.068
n 1(N 2)	σ*C 8 - H23	1.37	0.68	0.028
n 1(N 2)	σ*C 8 - H24	1.26	0.68	0.027
n1(N 1 - C 3)	σ*C 5 - H15	1.04	1.11	0.030
n 1(N 1 - C 3)	σ*C 5 - H15	1.04	1.11	0.030
n 1(N 1 - C 3)	σ*C 6 - H16	1.02	1.11	0.030
n 1(N 1 - C 5)	σ*C 3 - H10	1.14	1.11	0.032
n 1(N 1 - C 5)	σ*C 6 - H18	1.21	1.11	0.033
n 1(N 2 - C 4)	σ*C 7 - H21	1.02	1.11	0.030

4.2 Bonding Analysis

NBO analysis is executed in order to quantifying resonance structure contributions to the molecule and also provides an efficient method to study intra-molecular charge transfer interactions, rehybridization and delocalization of electron density within the molecule. NBO analysis was performed at B3LYP/6-31G(d,p) level to reveal the delocalization of electron density of NTE and Second order perturbation theory analysis of Fock matrix in NBO basis as given in Table 2. From the Table 2, the transitions has been confirmed by the charge transfer lone pain with anti-bonding orbitals of n1 (N1) $\rightarrow \sigma$*(C3– H9); n1 (N1) $\rightarrow \sigma$*(C6– H17); n1 (N1) $\rightarrow \sigma$*(C1-H17) and n1(N2) $\rightarrow \sigma$*(C4-H11) with the stabilization energies 8 kcal/mol. Likewise some more transitions also given in Table 2. From these values, the transitions that contribute to intra-molecular charge transfer, and therefore, to the stabilization of the system, are mainly due to orbital overlap between the bonding (σ) $\rightarrow$ antibinding (σ*) and lone pair (n) $\rightarrow$ antibinding (σ*) orbitals.

4.3 Electronic Spectral Analysis

The Highest Occupied Molecular Orbitals (HOMO) and the Lowest Unoccupied Molecular Orbital (LUMO), along with the HOMO-LUMO gap which is plot in DOS spectrum of the NTE is shown in Fig. 2. Generally, the intra-molecular charge transfer occurs from side to side the excitation of an electron from the HOMO to the LUMO. From Fig. 2, the HOMO LUMO plots can be seen the intra-molecular charge transfer. HOMO energy is 5.6139 eV, LUMO energy is -1.1186 eV and the energy gap ($E_{HOMO-LUMO}$) is 4.4953 eV which low energy gap ensures the biological activity of NTE.
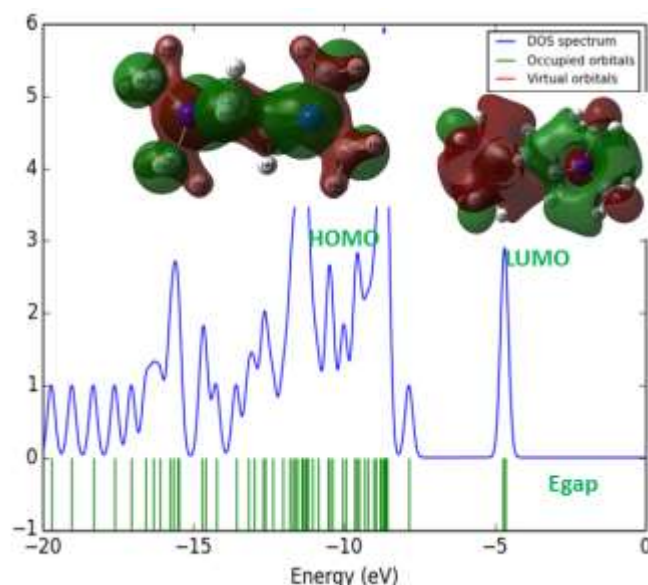
Table 2 Bonding Analysis of NTE

Donor (i)	Acceptor (j)	E(2)[a] (kcal/mol)	E(j)-E(i)[b] (a.u)	F(ij)[c] (a.u)
n 1(N 1)	σ*C 3 - C 4	1.86	0.66	0.032
n 1(N 1)	σ*C 3 - H 9	8.44	0.66	0.068
n 1(N 1)	σ*C 5 - H13	1.37	0.68	0.028
n 1(N 1)	σ*C 5 - H14	8.47	0.65	0.068
n 1(N 1)	σ*C 5 - H15	1.26	0.68	0.027
n 1(N 1)	σ*C 6 - H16	1.30	0.68	0.027
n 1(N 1)	σ*C 6 - H17	8.54	0.65	0.068
n 1(N 1)	σ*C 6 - H18	1.34	0.68	0.028
n 1(N 2)	σ*C 3 - C 4	1.86	0.66	0.032
n 1(N 2)	σ*C 4 -	8.44	0.66	0.068

Fig 2 HOMO- LUMO plots with its DOS spectrum

The UV-Vis spectrum of NTE is shown in Fig. 3 and the UV-vis wavelength with their contributions of NTE are given in Table 3 which is characterized by the presence of an absorption band in the region between 250 and 400 nm. The observed absorption value at λ_{max} at 300 nm is attributed to the transition $n \rightarrow \sigma^*$ where this transition corresponds to the HOMO $\rightarrow$ LUMO boundary orbital. The band gap value is correlates with the HOMO LUMO energy gap.

Table 3 UV-vis wavelength and their contributions of NTE

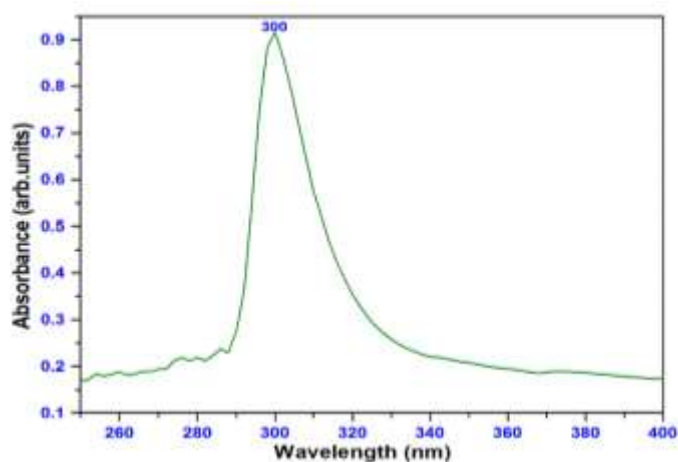| Energy (cm^{-1})	Experimental			Theoretical	Osc. Strength	Symmetry	
	Wavelength (nm)	Band gap	Wavelength (nm)	Band gap			
38597	300	4.133	299	4.1471	0.0009	Singlet-A	HOMO LUMO (99%)
38624			258	4.8062	0.0009	Singlet-A	HOMO-1 LUMO (99%),
39615			252	4.9206	0.0447	Singlet-A	HOMO-1 LUMO (99%)

Fig 3 UV Spectrum of NTE

4.4 Vibrational Spectral Analysis

The vibrational spectral assignments have been performed by NCA using the scaled quantum mechanical force field methodology. The simulated and experimental FT-IR along with FT-Raman spectra are publicized in Fig. 4 and 5 respectively. The thorough vibrational assignments with PED contributions are presented in Table 4. The detailed vibrations of NTE are given below:
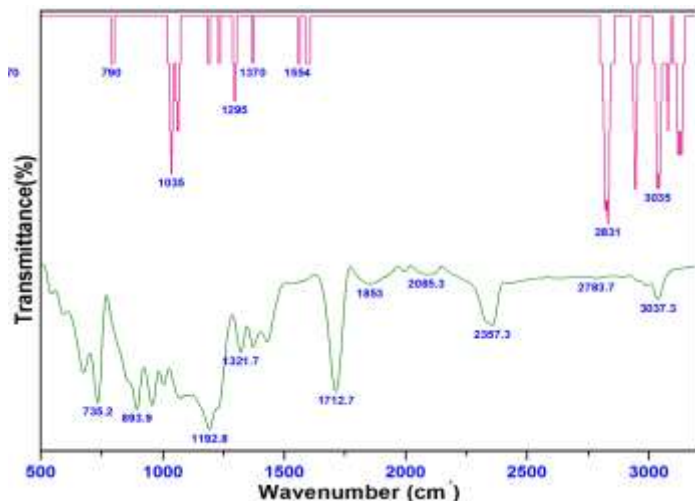

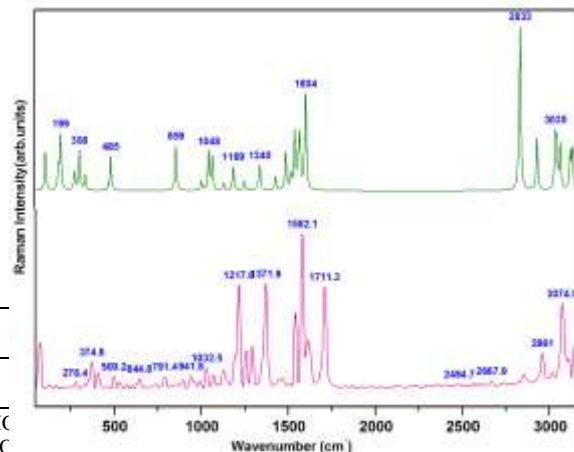**Fig 4 (A) Experimental (B) Simulated IR Spectra**

Fig 5 (A) Experimental (B) Simulated Raman Spectra

4.4.1 CH$_2$ group vibrations

Generally, the asymmetric and symmetric CH$_2$ stretching vibration in amino acids are detected in the region 3100-3000 cm^{-1} and 3000-2900 cm^{-1} respectively [12]. The symmetric stretching vibration is scaled at 3078 and 3063 in addition asymmetric CH$_2$ stretching vibration is observed at 2961 cm^{-1} corresponding scaled at 2944 cm^{-1} and 2930 cm^{-1}. The other bending and torsions of methylene are given in Table 4.

4.4.2 CH$_3$ group vibrations

Typically, the CH$_3$ asymmetric and symmetric stretching vibrations in the alkyl group occur at lower frequencies for instance 3010-2900 cm^{-1} and 2950-2850 cm^{-1} respectively when compared to that of the aromatic C-H stretching vibrations (3150–3000 cm^{-1}) [13,14]. CH$_3$ asymmetric stretching vibrations are observed as strong bands in Raman at 3241, 3144 and 3111 cm^{-1} and in IR at 3037 as a strong band and 2990 cm-1 as a weak band these corresponding scaled values are good agreement with scaled values and the symmetric stretching vibrations also are given in Table 4. The observed blue shift in stretching frequency is due to the formation of intra-molecular C–H…N hydrogen bonding. The increases in intensity of these bands are due to the methyl group are attaches with nitrogen having electron–donor properties.

Normally, CH$_3$ asymmetric and symmetric bending vibrations seem to be in the region 1470 -1440 cm^{-1} and 1390 - 1370 cm^{-1} respectively [18]. The asymmetric vibrations are observed in Raman at 1614, 1582, 1542 and 1472 cm^{-1} in addition symmetric bending vibrations are observed in IR at as a strong band at 1322, 1192 cm^{-1} with Raman counterpart as strong bands observed at 1295, 1258 and 1217 cm^{-1}. All these modes are good agreeing to scaled values are given in Table 4.

4.4.3 C-N and C-C Vibrations

The characterization of C-N stretching mode is mixing with vibrations such as C-C stretching, C-H in-plane , and CH$_3$ vibrations. The C-N stretching frequencies for some classes of compounds have been carried at the 1495-1028 cm^{-1} region. Chis *et al* . [19], for 2-fluoro benzamide at 1408 and 1096 cm^{-1} was observed by Krishnakumar et al . [20] In NTE, this mode is observed as medium in IR intensity at 1072 cm-1 and in Raman at 1073 and 1032 cm^{-1}. The C-C stretching vibration is observed at 1004 cm^{-1} in IR and in Raman at 965 cm^{-1}.

Table 4 Vibrational assignments of NAA

Calculated Wavenumber (cm⁻¹)	Observed fundamentals (cm⁻¹)		Assignment with PED%
	IR	Raman	
3134		3241s	MLOS (73), MLIS (26)
3134		3144s	MLOS(64), MLIS(36)
3121			MLOS(58), MLIS(40)
3121		3111w	MLIS(56), MLOS(43)
3078			MNSS(50), MNAS(44)
3063			MNAS(52), MNSS(45)
3044	3037s		MLIS(78), MLSS(11), MLOS(10)
3043			MLOS(58), MLIS(31), MLSS(11)
3035			MLIS(46), MLOS(38), MLSS(12)
3035	2990w		MLIS(53), MLOS(34), MLSS(12)
2944		2961s	MNAS(52), MNSS(47)
2930			MNSS(53), MNAS(46)
2833			MLSS(85), MLIS(10)
2832			MLSS(85), MLIS(9), MLOS(6)
2821			MLSS(85), MLIS(9), MLOS(5)
2821			MLSS(85), MLIS(9), MLOS(5)
1605		1614s	MLOB(85)
1604			MLOB(66), δMN (23)
1595			MLOB(87), MLIR(7)
1593			MLOB(87), MLIR(7)
1581		1582vvs	δMN(83)
1569			MNS (67), MLOB(22)
1561			MLIB(82), MLOR(8)
1560			MLIB(86), MLOR(8)
1542		1542vs	MLIB(79), MLOR(10)
1542			MLIB(82), MLOR(11)
1520			MLSD(96)
1520			MLSD(92)
1490			MLSD(85), δMN (11)
1489		1472vs	MLSD(88)
1431	1431m	1445w	ωMN (64), MNT (11), CN (9)
1371	1343m	1372vvs	ωMN (76), CC (11), CN (10)
1341			τMN (71), ωMN (6), MLOR (6)
1332			MLOR(29), MLIR(22), CN (20), CNSD(11), MLIB(10),
1328		1322s	MLOR(32), MLIR(22), CN (20), CNSD(12), MLIB(10)
1297		1295s	MNR (35), CN (17), MLOR(15), MLIR(11), CNR (10)
1282			MNT (35), MNW (23), MLIR(11), MLOR (10)
1251		1258s	MLIR(55), MLOR(36), MLOB(10)
1234		1217vs	MLIR(54), MLOR(20), MNT (13), CN (7)
1192	1192		MLOR(33), MLIR(31), ωMN (13), CN (8)
1189			MLIR(39), MLOR(33), CN (7)
1186			MNR (50), MLOR(24), MLIR(14), MNT (7)
1133		1129m	MLOR(49), MNT (24), MLIR(16)
1068	1072m	1073m	υCN (80), MLOR(10), MLIR(6)
1062			υCN (69), CC (16), MLOR(7)
1048			υCN (71), MLOR(

			12), MLIR(7)
1037		1032m	υCN (53), MLOR(13), CCPS(12), MNR (7),
1006	1004s	965w	υCC (48), υCN (24), CCPS (19)
859	857vs	869	υCN (76), CCPS (16)
838		841	ρMN (61), υCN (14), τMN (12), τMN (11)
796	735vvs	791m	υCN (74), MNR (16)
485		500s	CNSD (54), CCPS (18), υCN (11)
472		453vvw	ρCN (28), CCPS (25), CNSD (21), ωCN (16)
419		411vs	CNSD (69), ρCN (12),
371		375vvs	ωCN (57), ρCN (19), CNSD
342		338w	ωCN (46), ωCN(34)
308			ρCN (25), CCPS(24), CNSD(23), υCN (18)
280		278m	ωCN (58), CNSD(23), ρCN (11),
204		208w	ρCN (46), ωCN (34)
199			τMN (87), τML (10)
187			τMN (48), CNW (17), τML (11), CCPS(10), MNR (7)
184		170w	τMN (60), τML (20),
144		131w	CCPS(45), CNW (19), CNSD (14), τML (12), CNR (10)
112			τML (92)
79		76s	τML (83), ρCN(10)
10			τML (68), TMN (17), CNSD(11)

vw-very weak; w-weak; m-medium; vs-very strong; s-strong;ν-stretching; SS- symmetric stretching; AS-asymmetric stretching; IP- in-plane stretching; OP- out of plane stretching; TD- trigonal deformation; AD- asymmetric deformation; ADO-out of plane asymmetric deformation; PU-Puckering; AT-asymmetric torsion; ATO-out-of plane asymmetric torsion; ML- Methyl; MN- Methylene;ρ - Rocking; δ-Scissoring;ω-Wagging; γ-Twisting

4.5 Charge Analysis

4.5.1 Atomic charge analyses

The atomic charge of a molecule is an essential chemical property and used to elucidate in chemical reactivities the electronegativity equalization, electronic structures, charge transfer mechanism. Atomic charges of NTE are presented in Table 5. Atoms C5 and C8 atom have larger negative charge among all carbon atoms which confirms these atoms involve in the intra-molecular hydrogen bonding interactions. From The Table 5, one hydrogen atom from each methyl group higher than other two hydrogens are reasonably suitable for the intra-molecular interaction in solid states.

Table 5 Natural Charge of NAA

Atoms	Natural Charge	Atoms	Natural Charge	Atoms	Natural Charge
N1	-0.55717	H13	0.18898	N1	-0.55717
N2	-0.55717	H14	0.16004	N2	-0.55717
C3	-0.16938	H15	0.19189	C3	-0.16938
C4	-0.16938	H16	0.19027	C4	-0.16938
C5	-0.35549	H17	0.15922	C5	-0.35549
C6	-0.34983	H18	0.19010	C6	-0.34983
C7	-0.34983	H19	0.19010	C7	-0.34983
C8	-0.35549	H20	0.15922	C8	-0.35549
H9	0.16444	H21	0.19027	H9	0.16444
H10	0.18692	H22	0.16004	H10	0.18692
H11	0.16444	H23	0.18898	H11	0.16444
H12	0.18692	H24	0.19189	H12	0.18692

4.5.2 Electrostatic Potential Analysis

The Molecular Electrostatic Potential (MEP) map is a qualitative explanation of nucleophilic and electrophilic reaction sites. The MEP map of the NTE molecule is also displayed in Fig. 6. Thus, the most negative region (Red and blue) is that of the around nitrogen atoms which are whereas the most positive(white and green) is the methyl group. This contributes to a cooperative effect charge transfer providing additional stability to the system.
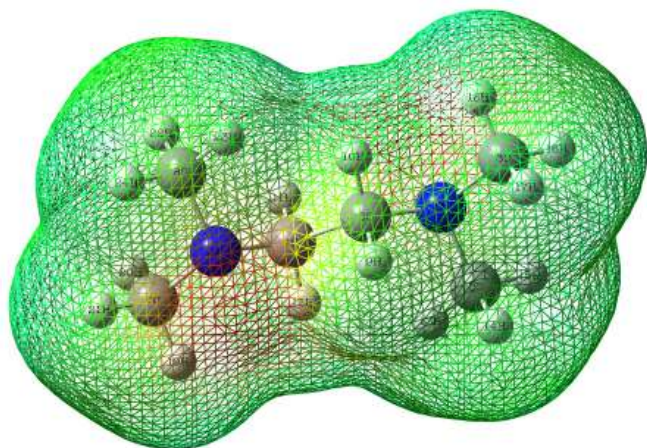
Fig 6 Electrostatic Potential Map

4.6 ELF AND LOL Analysis

ELF is a measure of the possibility of outcome an electron in the vicinity of a reference electron positioned at a given point and has the same spin [21,22]. High ELF values around 0.9e are colored red the series fall away through green to blue for middle ELF values ~0.5e. The lowest value is represented by blue. Furthermore, a n-σ* anomeric effect is estimated between the lone pair nitrogen atoms [23]. This ought lead to a deformation of the ELF sharing around the methyl groups. The 2D plot of ELF and LOL in the hydrogen bonding region is shown in Fig. 7. The monosynaptic lone pair regions of N occupy more space and then it can attract the H atom of methyl group, leading to hydrogen bonding.
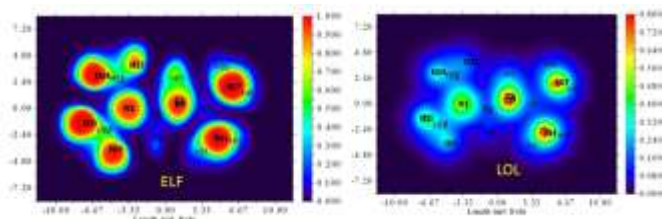

Fig 7 Colour filled Electron Localization Functionofhydrogen bonding region in

LOL is based on comparing local non-interacting kinetic energy density with uniform electron gas density (Causà et al., 2015). LOL values are less than 0.5, which exhibits the non-covalent interactions. The covalent regions are seen between hydrogen and nitrogen atoms, indicated by red color with high LOL value, the electron depletion regions between valence shell and inner shell are shown by the blue circles around the carbon and oxygen nuclei. LOL conveys a more significant and perfect portrait than ELF.

4.7 Reduced Density Gradient Analysis

Non-Covalent interaction analysis is frequently used to evaluate intra and inter-molecular non-covalent interactions. The reduced density gradient (RDG) analysis is relied on electron density and its derivatives, purely be responsible for the region of these interactions besides their pictorial reference. A graphical representation offers beneficial information on the effectiveness and nature of interactions. The repulsive, attractive, and van der Waals interactions correspond to sign(λ2) ρ> 0, sign(λ2) ρ< 0 and sign(λ2) ρ≈0, respectively [24-25]. 2D scatter and Isosurface density plots

illustrating the non-bonded interactions of RDG isosurface are shown in Fig.8.

The RDG plot between the negative area -0.045 to -0.025 a. u. highlighted by blue colour depicts a more favourable interaction due to strong hydrogen bonds. The red colour in the centre of the methyl group around nitrogen atoms indicate steric effect, which is also visible in the scatter plot in the positive 0.015 to 0.03 a. u. areas. Green color reveals van der Waals interactions between the hydrogen atoms, which is also seen from RDG plot between regions -0.02 to 0.005 a. u.
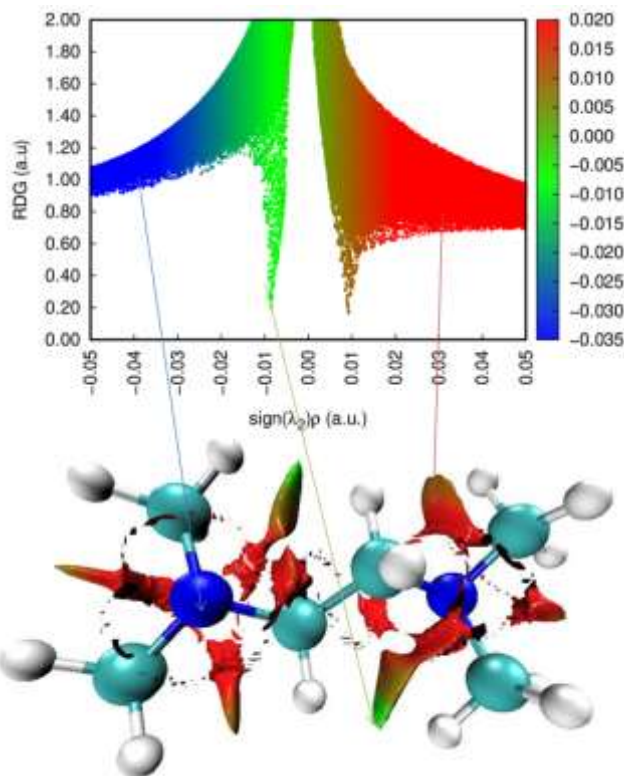

Fig 8 Reduced Density Gradient Analysis

4.8 Antimicrobial Activity

The NTE molecule was screened for its in vitro antimicrobial activity against bacterial and fungal strains by agar well diffusion method. The activity was determined by measuring the inhibition zone diameter values (mm) of the investigated compound. The antimicrobial activity test for microbial strains were measured and mentioned in the Tables 6. and the photographed are shown in Figure 9. The molecule NTE was tested for its antimicrobial activity against human pathogens of clinical isolates (*Salmonella paratyphi, Shigella sp., Staphylococcus aureus, Streptococcus pyogenes and Klebsiella pneumonia*).

Fig 9 Antimicrobial Activity of NTE

NTE showed a maximum inhibition of zone diameter 36mm by *Klebsiella pneumonia.* This is followed by *Staphylococcus aureus, Streptococcus pyogenes* and *Staphylococcu saureus* with a diamter shows resistant to NTE. Comparative study results in a high degree zone of inhibition seen in streptomycin than ciprofloxacin. Penicillin G showed very less zone of inhibition of the selected pathogens. *Klebsiella. pneumoniae* can be treated with antibiotics if the infections are not drug-resistant. These results clearly indicate that the compound has antimicrobibacterial activities against the tested organisms. The presence of methyl group is responsible for the antibacterial action.

Table 6 Antimicrobial activity of NTE

Sl.No	Microorganisms	Zone of inhibition (diameter in mm)		
		Ciprofloxacin	Streptomycin	Penicillin G
1	*Salmonella paratyphi*	20	6	6
2	*Shigella spp.*	20	6	6
3	*Staphylococcus aureus*	20	20	6
4	*Streptococcus pyogenes*	20	16	6
5	*Klebsiella pneumonia*	36	17	7

4.9 Drug likeness

An extensive choice of potential medicinal applications fort this substance showed a drug-likeness test on the SwissADME [30] online platform. According to the rule of thumb, orally absorbed drugs ought to have the tendency to obey Lipinski's rule of five. The rule was derived from an analysis of compounds from the World Drugs Index database aimed at identifying features that have been important in making a drug orally active. It has been found that the factors

concerned involved numbers that are multiples of five: [26–31]. All these expected values as given in Table 7 are satisfied within the acceptable range. A molecule can be a suitable candidate for drug and it is clear that NTE is a good candidate to be utilized as a drug because it satisfies four Lipinski rules.

Table 7 Drug likeness parameters calculated for title molecule

Descriptors	Calculated	Expected
Molecular mass(Dalton)	116	<500
Hydrogen bond donor	0	<5
Hydrogen bond acceptor	2	<10
Log P	0.1096	<5
Molar refractivity	42.1079	40-130

5. Conclusion

A detailed exploration of the structural, vibrational, electronic, and biological properties of NTE was analysed using spectroscopic techniques and DFT computation methodology. The HOMO-LUMO energy gap is 5.186 eV indicating that the molecule would be stable and bioactive. The reactive areas of the molecule are schematically depicted using MEP and it is highly electrophilic around the nitrogen atoms, enabling it to interact with proteins produced from amino acids. The antibacterial test supports vital antibacterial efficacy against the *Klebsiella pneumonia.* that causes urinary tract infections, pneumonia, and meningitis. NTE is appropriate to be used as an antibacterial therapeutic because it vividly matches the Lipinski rule of five and also shows inhibitory action against the tested bacterial strains.

References

[1]P.S. Coelho,J.C. Lewis, in Comprehensive Organic Synthesis (Second Edition), 2014

[2] Lian J, Wang J, Sun HF, Lin DZ, Liu H, Yao Xue Xue Bao, Application of methyl in drug design].. 2013, 48(8),1195-208.

[3] Massa, A. Recent Advances in the Chemistry of Active Methylene Compounds. 2012, 16, 2159–2169.

[4]M.J. Frisch, G.W. Trucks, H.B. Schlegel, G.E. Scuseria, M.A. Robb, J.R. Cheeseman, G. Scalmani, V. Barone, B. Mennucci, G.A. Petersson,H. Nakatsuji, M. Caricato, X. Li, H.P. Hratchian, A.F. Izmaylov, J. Bloino,G. Zheng, J.L. Sonnenberg, M. Hada, M. Ehara, K. Toyota, R. Fukuda,J. Hasegawa, M. Ishida, T. Nakajima, Y. Honda, O. Kitao, H. Nakai, T. Vreven,J.A. Montgomery Jr., J.E. Peralta, F. Ogliaro, M. Bearpark, J.J. Heyd, E. Brothers,K.N. Kudin, V.N. Staroverov, T. Keith, R. Kobayashi, J. Normand,K. Raghavachari, A. Rendell, J.C. Burant, S.S. Iyengar, J. Tomasi, M. Cossi,N. Rega, J.M. Millam, M. Klene, J.E. Knox, J.B. Cross, V. Bakken, C. Adamo,J. Jaramillo, R. Gomperts, R.E. Stratmann, O. Yazyev, A.J. Austin, R. Cammi,C. Pomelli, J.W. Ochterski, R.L. Martin, K. Morokuma, V.G. Zakrzewski,G.A. Voth, P. Salvador, J.J. Dannenberg, S. Dapprich, A.D. Daniels, O. Farkas, J.B. Foresman, J.V. Ortiz, J. Cioslowski, D.J. Fox, Gaussian 09, Revision C.02,Gaussian Inc., Wallingford CT, 2010.

[5] T. Sundius, Vib. Spectrosc 29 (2002)89–95,

[6] T. Sundius, J. Mol. Struct. 218(1990) 321–326, https://doi.org/10.1016/0022-2860 (90)80287-T.

[7] G. Rauhut, P. Pulay, J. Phys. Chem. 99 (1995) 3093–3100.

[8] E.D. Glendening, A.E. Reed, J.E. Carpenter, F.Weinhold, NBO Version 3.1, TCI, University of Wisconsin, Madison, 1998.

[9] T. Lu, F. Chen, Multiwfn: a multifunctional wave function analyser, J. Comput. Chem. 33 (2012) 580-592.

[10] B. Fathima Rizwana, J. Christian Prasanaa, S. Muthu, Christina Susan Abraham, Comp.Biology and Chemistry 78 (2019) 9–17,

[11] W. Humphrey, A. Dalke, K. Schulten, VMD: visual molecular dynamics. J. Mol. Graph. 14(1996) 33–38.

[12] N.B. Colthup, L.H. Daly, S.E. Wiberley, Introduction to Infrared and Raman Spectroscopy, Academic Press, New York, 1990.

[16] J. Swaminathan , M. Ramalingam , V. Sethuraman , N. Sundaraganesan , S. Sebastian , Spectrochim. Acta Part A 73 (2009) 593–600 .

[17] B.C. Smith, Infrared Spectral Interpretation: A Systematic Approach, CRC Press, Washington, DC, 1999.

[18] F.R. Dollish, W.G. Fateley, F.F. Bentley, Characteristic Raman Frequencies of Organic Compounds, John Wiley & Sons, New York, 1997.

[19] V. Chis, Chem. Phys. 300 (2004) 1-11

[20] V. KrishnakumarS. Muthunatesan, Spectrochimica Acta Part A 65 (2006) 818–825

[21] A.D. Becke, K.E. Edgecombe, J. Chem. Phys. 92 (1990) 5397.

[22] A. Savin, 0 Jepsen, J. Flad, O.K. Andersen, H. Preuss, H.G. von Schnering, Angew.

Chem. 31 (1992) 187.

[23] Andreas Savin, Reinhard Nesper, Steffen Wengert, Thomas E. Fassler, Angew. Chem. Int. Ed. Engl. 36 (1997) 1808-1832.

[24] G. Saleh, C. Gatti, L. Lo Presti, Comput. Theor. Chem. 998 (2012) 148–163,

[25] E.R. Johnson, S. Keinan, P. Mori-Sanchez, J. Contreras-Garcia, A. J. Cohen, W. Yang, J. Am. Chem. Soc. 132 (2010) 6498–6506,

[26] C.A. Lipinski, Drug Discov. Today Technol. 1 (4) (2004) 337–341.

[27] W.P. Walters, M.A. Murcko, Adv. Drug Deliv. Rev.54 (3) (2002) 255–271.

[28] D.E. Clark, S.D. Pickett, Drug Discov. Today 5 (2) (2000) 49–58.

[29] S. Tian, J. Wang, Y. Li, L. Li, T. Hou Xu, Adv. Drug Deliv. Rev. 86 (2015) 2–10.

[30] O. Ursu, A. Rayan, A. Goldblum, T. Oprea, Rev. Comput. Mol. Sci 5 (2011) 760–781.

[31] W.J. Egan, W.P. Walters, M.A. Murcko, Curr. Opin. Drug Discovery Develop. 5(4) (2002) 540–549.